DNA synthesis by Pol η promotes fragile site stability by preventing under-replicated DNA in mitosis

Valérie Bergoglio,[1,2] Anne-Sophie Boyer,[1,2] Erin Walsh,[3] Valeria Naim,[4] Gaëlle Legube,[2,5] Marietta Y.W.T. Lee,[6] Laurie Rey,[1,2] Filippo Rosselli,[4] Christophe Cazaux,[1,2] Kristin A. Eckert,[3] and Jean-Sébastien Hoffmann[1,2]

[1]Equipe labellisée Ligue Contre le Cancer 2013, INSERM Unit 1037, ERL5294 Centre National de la Recherche Scientifique (CNRS), Cancer Research Center of Toulouse (CRCT), BP3028, CHU Purpan, 31024 Toulouse, France
[2]Université Paul Sabatier, University of Toulouse III, F-31062 Toulouse, France
[3]Department of Pathology, Pennsylvania State University College of Medicine, Hershey, PA 17033
[4]University Paris-Sud, UMR8200 CNRS, Institut Gustave Roussy, 94805 Villejuif, France
[5]Laboratoire de biologie cellulaire et moléculaire du contrôle de la prolifération (LBCMCP), CNRS, University of Toulouse, F-31077 Toulouse, France
[6]Department of Biochemistry and Molecular Biology, New York Medical College, Valhalla, NY 10595

Human DNA polymerase η (Pol η) is best known for its role in responding to UV irradiation–induced genome damage. We have recently observed that Pol η is also required for the stability of common fragile sites (CFSs), whose rearrangements are considered a driving force of oncogenesis. Here, we explored the molecular mechanisms underlying this newly identified role. We demonstrated that Pol η accumulated at CFSs upon partial replication stress and could efficiently replicate non-B DNA sequences within CFSs. Pol η deficiency led to persistence of checkpoint-blind under-replicated CFS regions in mitosis, detectable as FANCD2-associated chromosomal sites that were transmitted to daughter cells in 53BP1-shielded nuclear bodies. Expression of a catalytically inactive mutant of Pol η increased replication fork stalling and activated the replication checkpoint. These data are consistent with the requirement of Pol η–dependent DNA synthesis during S phase at replication forks stalled in CFS regions to suppress CFS instability by preventing checkpoint-blind under-replicated DNA in mitosis.

Introduction

During S phase of the cell division cycle, the genome must be precisely duplicated, with no regions left under-replicated so genomic integrity can be maintained. This is an intrinsically challenging task, even apart from environmental insults, because progression of replication forks can be slow or problematic at specific genomic loci (Tourrière and Pasero, 2007; Branzei and Foiani, 2010). Natural replication barriers include non-B structured DNA, repetitive sequences, protein–DNA complexes, and DNA lesions (Branzei and Foiani, 2010). Non-B DNA structures formed within expanded microsatellites stall replication fork progression in vivo, and a causal link between non-B DNA structure formation, replication fork stalling, and genome instability has been demonstrated in microsatellite expansion disease etiology (Pearson et al., 2005; Mirkin, 2007). If active replication origins are deficient in the vicinity of a stalled fork, this increases the possibility of incompletely replicated regions or unresolved replication intermediates, which may evolve into chromosomal breakage. Chromosomal common fragile sites (CFSs) have received particular interest in recent years because they are frequently sites of structural rearrangement in tumors (Durkin and Glover, 2007; Bignell et al., 2010) and their instability constitutes one of the earliest events of oncogenic transformation (Bartkova et al., 2005; Gorgoulis et al., 2005). CFSs are typically relatively large (several hundred kb) regions of chromosomal DNA that can be replicated in late S phase. Unlike rare fragile sites, which are caused by expansions of tandem repeat sequences, expanded repeat sequences have not been identified

V. Bergoglio and A.-S. Boyer contributed equally to this paper.

E. Walsh and V. Naim contributed equally to this paper.

Correspondence to Jean-Sébastien Hoffmann: jseb@ipbs.fr

Abbreviations used in this paper: APH, aphidicolin; CFS, common fragile site; ChIP, chromatin immunoprecipitation; PIP, PCNA-interacting protein; Pol η, polymerase η; RPA, replication protein A; TLS, translesion synthesis; UBZ, ubiquitin-binding domain; WT, wild type; XPV, variant form of xeroderma pigmentosum.

The Rockefeller University Press $30.00
J. Cell Biol. Vol. 201 No. 3 395–408
www.jcb.org/cgi/doi/10.1083/jcb.201207066

in CFSs (Durkin and Glover, 2007). However, several CFSs have been shown to contain AT-rich regions predicted to generate islands of increased DNA flexibility (Lukusa and Fryns, 2008), and a recent study identified G-negative chromosomal banding patterns, increased distance from the centromere, CpG island depletion, and the presence of Alu repeats (associated with mononucleotide repeat sequences) as genomic predictors of CFSs (Fungtammasan et al., 2012). Despite the importance of CFSs as sites of structural rearrangement in early stages of cancer development, the regulation of CFS stability is still not fully understood. Recent evidence has shown that the fragility of specific CFSs can be due to a paucity of replication initiation events (Letessier et al., 2011) or can be induced by the inability to activate additional origins upon fork stalling (Ozeri-Galai et al., 2011). Because CFSs are known to display gaps or breaks on metaphase chromosomes after partial inhibition of the replicative DNA polymerases, current models propose that instability arises as a consequence of challenges to fork movement, including the presence of subregions with the potential to form non-B DNA secondary structures (Schwartz et al., 2006) or encounters with the transcription machinery (Helmrich et al., 2011). CFS instability is enhanced in ATR-deficient cells (Casper et al., 2002) or when Chk1 activity is compromised (Durkin et al., 2006), suggesting that the ATR pathway stabilizes replication forks stalled within fragile site sequences to ensure replication and the completion of S phase while avoiding DNA breakage (Durkin and Glover, 2007). Several proteins involved in the recognition and processing of DNA damage contribute also to maintaining CFS stability, notably BRCA1, RAD51, FANCD2, MSH2, WRN, and BLM (Debatisse et al., 2012).

Unexpectedly, we recently discovered that a specialized translesion synthesis (TLS) DNA polymerase, Pol η, is also required for the suppression of CFS instability under conditions of unperturbed growth or upon replicative stress (low dose of aphidicolin [APH]; Rey et al., 2009). Thus far, Pol η was best known for its role in responding to genome damage that arises when a cell is exposed to an extrinsic genotoxic stress, such as UV irradiation. Patients with *POL H* gene mutations are affected by the variant form of xeroderma pigmentosum (XPV), a rare, autosomal, recessive human genetic syndrome associated with sun hypersensitivity, UV hypermutability, numerous skin abnormalities, and a high level of early and multiple skin cancers on sun-exposed sites of the body. This phenotype is consistent with the biochemical function of Pol η in supporting efficient TLS across one of the major UV-induced lesions, the cyclobutane thymine dimer (Masutani et al., 1999; McCulloch et al., 2004). We demonstrated that Pol η–depleted cells exhibit an elevated instability of a CFS, suggesting a new function of Pol η during normal DNA replication in unperturbed cycling cells or after partial inhibition of the replicative DNA polymerases (Rey et al., 2009). Here, we explored the mechanistic basis explaining how Pol η can be required for maintaining CFS stability during S phase. We found that Pol η is recruited to CFS regions and that Pol η acts during S phase at stalled forks to perform efficient DNA synthesis of non-B DNA structures within these regions, preventing persistence of under-replicated DNA in mitosis and its transmission to daughter cells.

Results

Pol η is recruited at CFS sequences

To evaluate whether Pol η–dependent CFS stability relies on a direct interaction of the polymerase at these sequences, we first investigated if Pol η binds to CFS regions by performing chromatin immunoprecipitation (ChIP) combined with quantitative real-time PCR (qPCR) targeted to CFSs. Because our previous findings indicated that Pol η depletion triggers FRA7H expression (translocations, amplifications, deletions) in U2OS cells under conditions of low replication stress, we performed the ChIP in FRA7H regions after treatment with a low dose of APH in U2OS cells stably expressing wild-type (WT) Pol η. The data indicate a modest but reproducible and significant enrichment of WT Pol η in genomic regions that map with two hot spots for DNA breakage within FRA7H, FRA7H.1, and FRA7H.2 (Fig.1, left panels; Mishmar et al., 1998; Schneider et al., 2008). We also found that WT Pol η can be recruited directly at another hot spot for DNA breakage within FRA16D (Fig. 1, bottom left). It has been shown that Pol η is highly mobile within replication foci in the nucleus of human cells (Sabbioneda et al., 2008). Therefore, we reasoned that the expression of an inactive form of Pol η would increase the polymerase residence time at replication forks as previously proposed (Sabbioneda et al., 2008). To test this hypothesis, we performed ChIP analysis in cells stably expressing a catalytically inactive form of Pol η (Dead Pol η), in which we have mutated to alanines two critical active site residues vital for catalytic activity (D115A and E116A), allowing the incoming nucleotide to bind but preventing the formation of the phosphodiester bond. We found a significantly greater enrichment of Dead Pol η compared with WT Pol η in FRA7H.1, FRA7H.2, and FRA16D (Fig.1, right panels; Fig. S1 A), supporting that the detection of Pol η at CFSs can be strengthened when the catalytic activity is defective.

Pol η can efficiently synthesize through structured non-B DNA at CFS sequences

One hypothesis for the recruitment of Pol η to CFSs is that Pol η directly performs DNA synthesis through structured or repetitive DNA sequences within CFSs, whose distortions might impede the elongation process by the replicative DNA polymerases. In this model, the stalled replicative DNA polymerase is replaced transiently by Pol η, which is capable of bypassing structured DNA similar to the TLS process, thus avoiding interruptions of fork progression. We tested this possibility by comparing polymerase synthesis profiles at the nucleotide level, in vitro, between purified recombinant human Pol η and the human four-subunit replicative Pol δ, on DNA sequences from FRA16D and FRA3B. The sequences analyzed are predicted to form non-B DNA secondary structures, and include: mononucleotide A/T repeats (bent DNA and slipped strand structures); AT/TA repeats (hairpin and slipped strand structures); and inverted repeats (IRs; hairpin structures). The progression of DNA synthesis through CFS-derived templates was quantified by comparing regions of non-B DNA potential to a control sequence devoid of non-B DNA structure potential. Specific pausing/stalling sites for Pols δ and η were determined as previously established (Shah et al., 2010).

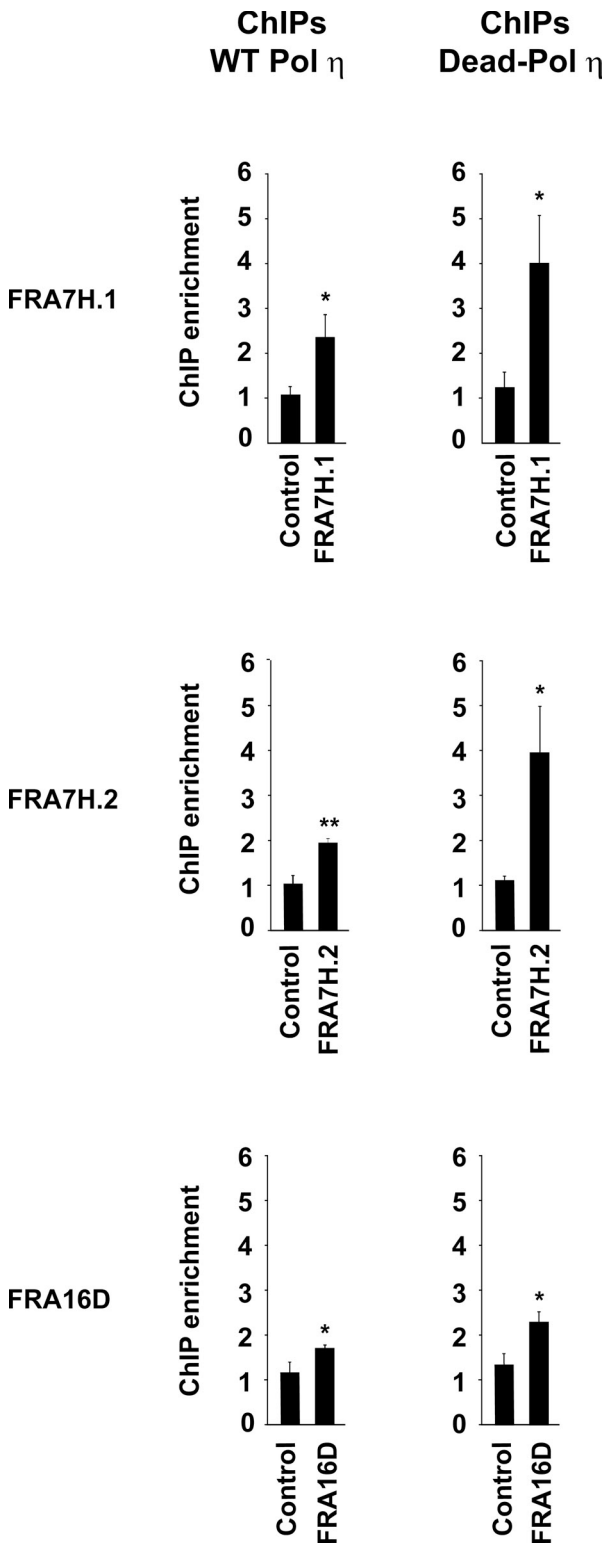

Figure 1. **Pol η accumulates at CFSs after replication stress.** U2OS cells stably expressing WT Pol η (left panels) or Dead-Pol η (right panels) were exposed to 0.2 μM APH for 24 h and analyzed by chromatin immunoprecipitation (ChIP) followed by quantitative PCR for accumulation of WT Pol η and Dead Pol η at the indicated CFSs (FRA7H.1, FRA7H.2, and FRA16D) or control genomic regions (DHFR, GAPDH). Fold increase of chromatin immunoprecipitation (ChIP) over input DNA was calculated as a ratio between mock and Pol η for each replicate. Data are presented as mean values of three independent experiments ± SEM. The statistical significance of Pol η enrichment at CFSs in comparison to DNA control region was assessed using *t* test. P-values for ChIPs were as follows: P = 0.033 for FRA7H.1; P = 0.004 for FRA7H.2; P = 0.048 for FRA16D (WT Pol η) and P = 0.030 for FRA7H.1; P = 0.023 for FRA7H.2; and P = 0.021 for FRA16D (Dead-Pol η).

We observed no significant pause sites for Pol δ or Pol η throughout the CFS control template, and measured no statistically significant difference between the two polymerases in percent transit at any time point analyzed (Fig. 2 A; $P > 0.05$). Using the same reaction conditions, both Pols δ and η undergo pausing throughout the A_{28} repeat on FRA16D template 1, likely due to the formation of bent DNA and/or slipped DNA strands (Fig. 2 B). However, Pol η pausing at the A_{28} repeat was substantially less than Pol δ, and after 15 min, Pol η synthesis efficiency (77%) was significantly greater than that of Pol δ (14.7%; $P = 0.0073$; Fig. 2 B). No significant pausing was observed by either polymerase at the interrupted TA_{24} repeat, possibly because the TA tract may not be sufficiently long to generate a stable hairpin (Dayn et al., 1991; Zhang and Freudenreich, 2007). Similarly, strong pausing was observed by Pol δ within the T_{19} repeat and at the interrupted inverted hairpin structure within the FRA16D template 2, whereas Pol η displayed only a brief pause at the base of the hairpin structure (Fig. 2 C). Quantitatively, the mean normalized percent transit for Pol δ reached only 16.4% on template 2, whereas Pol η showed significantly greater percent transit (91%) than Pol δ ($P = 0.0236$ and 0.0002, 5 and 15 min, respectively). We observed similar results in our analysis of pausing at the AT_{25} hairpin structure within the FRA3B template (Fig. 2 D), wherein Pol η displayed statistically significant enhanced synthesis compared with Pol δ ($P \leq 0.012$). Importantly, we found that addition of the PCNA clamp and RF-C clamp loader did not increase the progression of DNA synthesis by Pol δ on the CFS-derived templates (Fig. S1, B and C). Therefore, the majority of the DNA products produced by Pol δ are terminated within the CFS sequence. In contrast, the majority of Pol η DNA products are fully synthesized through the CFS sequences. Collectively, these findings suggest that the specialized Pol η is capable of more efficiently synthesizing past CFS non-B DNA structures, and might play a similar role in vivo.

One possible explanation for the observed efficient synthesis of CFS non-B DNA structures by Pol η is that the polymerase merely skips over the pause sites in an error-prone manner, resulting in deletion mutations. We analyzed Pol η fidelity by cloning and sequencing the products generated using the FRA16D template 2. Of the 105 clones analyzed, we detected only one large deletion mutation encompassing the predicted inverted repeat hairpin, and one smaller deletion near the hairpin (Fig. S1, E and F). Thus, over 99% of the Pol η reaction products retain the CFS sequence and do not contain deletion mutations (Fig. S1 E). As expected for the error-prone nature of the polymerase at the nucleotide level (Matsuda et al., 2001), however, signature Pol η base substitution mutations, particularly T→C transitions, were observed throughout the CFS region (Fig. S1 E). As a control, we also analyzed the minority of products from Pol δ reactions that had completed synthesis through the CFS sequence, both in the absence and presence of RF-C. No base

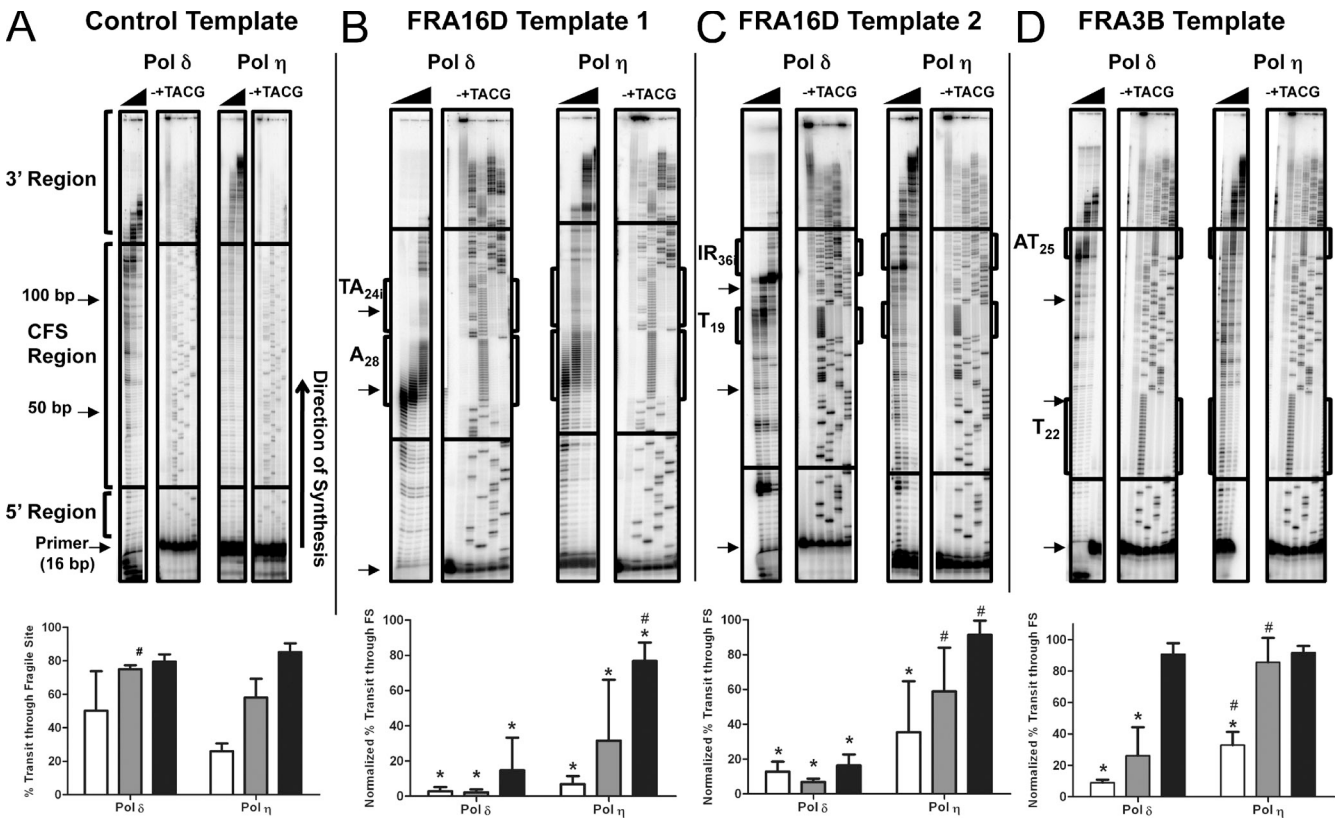

Figure 2. **Comparison of Pol δ and Pol η pausing within FRA16D and FRA3B non-B DNA sequence elements.** Primer extension reactions were performed as described in Materials and methods with 500 fmol-1 pmol human four-subunit Pol δ or 1 pmol human Pol η; in each panel is shown pausing gels for Pols δ and η (top) and quantification (bottom); black triangles represent 2-, 5-, and 15-min time points; −, no polymerase control; +, hybridization control; TACG, dideoxy sequencing ladder; horizontal lines indicate boundaries of CFS inserts. Sequences with predicted non-B DNA potential are outlined by brackets and annotated to the left of the gels. *, statistical significance ($P < 0.05$) between percent transit on the control template and template of interest for each Pol, determined by *t* test. #, statistical significance ($P < 0.05$) between normalized percent transit for Pol δ and η on the template of interest, determined by *t* test. Bars represent mean ± SD for three (Pol delta) or four (Pol eta) independent reactions. (A) Control CFS template; (B) FRA16D template 1; (C) FRA16D template 2; (D) FRA3B template. Pol δ and Pol η were assayed in parallel on the FRA3B template, so the same control samples and dideoxy sequencing ladder are shown for both in D.

substitution or large deletion mutations were observed among the 124 total clones analyzed (Fig. S1, D and E). These results show that although Pol η can efficiently synthesize through non-B DNA structures, it does so with an increased probability of producing base substitution errors, in contrast to the inefficient but more accurate synthesis by replicative Pol δ. This biochemical trade-off may be essential in ensuring complete replication of CFS non-B DNA structures in the cell.

Pol η deficiency leads to DNA replication delay and persistence of under-replicated regions in mitosis

Collectively, the results presented above are consistent with the idea that Pol η is recruited to CFSs during S phase in the absence of external stress or after inhibition of the replicative polymerases in order to replicate subregions containing structured DNA within CFSs. We speculate that deficiency of Pol η in human cells would result in under-replicated DNA at CFSs, contributing to their instability. To test this hypothesis, we were inspired by several recent studies showing that late completion of DNA replication at fragile sites is involved in their fragility, and that under-replicated regions or unresolved replication intermediates at fragile sites can escape checkpoint mechanisms, persist into mitosis as FANCD2-associated chromosomal sites, and be transmitted to daughter cells in 53BP1-shielded nuclear bodies (Chan et al., 2009; Naim and Rosselli, 2009; Harrigan et al., 2011; Lukas et al., 2011). Our findings that Pol η is recruited at CFSs and can efficiently synthesize subregions of CFSs prompted us to analyze the replication completion of these sites and the persistence of under-replicated regions in mitosis in Pol η–deficient cells. Unresolved replication intermediates at fragile sites in mitotic cells were identified by FANCD2 staining and the delayed replication of these regions was assessed with an in situ EdU incorporation assay. We analyzed EdU incorporation and FANCD2 spot persistence in Pol η–depleted U2OS (ShPolη) cells compared with the mock-depleted cells (ShCtrl) as well as in XP30RO cells from an XPV patient, compared with their Pol η–complemented counterpart (XPV+Pol η). For the delayed replication experiments, untreated or APH-treated cells were pulse-labeled in vivo with the thymidine analogue EdU for 45 min immediately before cell fixation, and mitotic cells at prometaphase and metaphase were analyzed for EdU incorporation. EdU incorporation observed in mitotic cells was confirmed by co-staining cells for phospho-histone H3 (Fig. S2 A). Most untreated mitotic cells were EdU negative, as expected to be the case in cells where DNA replication was completed before the EdU pulse, i.e., at least

Table 1. **EdU incorporation and FANCD2 spot frequency in untreated mitotic cells**

Cell lines	EdU-positive mitotic cells	EdU spots/cell	FANCD2-positive mitotic cells	FANCD2 spots/cell
U2OS ShCTRL	17 ± 3%	1.8	25 ± 4%	2.2
U2OS ShPolη	25 ± 4%	2	37 ± 4%	2.2
XPV+Polη	9 ± 2%	1.1	31 ± 4%	2.3
XPV	14 ± 3%	1.7	38 ± 4%	2.5

Asynchronously growing cells were labeled with EdU for 45 min, fixed, and stained with a FANCD2-specific antibody. Mitotic cells at prometaphase and metaphase presenting an EdU signal or discrete FANCD2 staining (EdU or FANCD2 spots) were scored as positive. Data are the mean ± standard errors from three independent experiments (n = 150).

45 min before mitosis. However, we could detect one or two discrete EdU spots in some of the mitotic cells (17 ± 3% of mock-depleted vs. 25 ± 4% of Pol η–depleted cells and 9 ± 2% of XPV+polη vs. 14 ± 3% of XPV; Table 1). Most of the EdU spots coincided with or were adjacent to the FANCD2 mitotic spots (Fig. 3 A), indicating that active DNA synthesis takes place in the FANCD2/EdU-positive sites within 45 min of metaphase, i.e., in late G2 or early M. Next, we analyzed the EdU incorporation and FANCD2 spot frequency after inducing a low level of replicative stress (200 nM APH). FANCD2 monoubiquitination in response to APH treatment was similar in Pol η–proficient and –deficient cells, indicating no obvious defect in replicative stress response (Fig. S2 B). The frequency of both EdU- and FANCD2-positive mitotic cells increased after APH treatment. However, deficiency of Pol η induced a reproducible shift toward mitotic cells with a higher number of EdU and FANCD2 spots, with a significant increase of mitotic cells presenting >40 or >20 EdU spots (Pol η–depleted cells and XPV, respectively) and >40 FANCD2 spots (Fig. 3 B), indicating a delay in replication completion and an increased persistence of late replication intermediates after APH treatment in the absence of Pol η (Fig. 3 B). These data support the notion that completion of CFS replication can occur in late G2-M, notably within 45 min of metaphase. Replication completion is further delayed in the presence of APH, leading to an increased occurrence and frequency of late replicating regions. This phenotype is exacerbated in the absence of Pol η, suggesting that a delayed replication completion and persistence of replication intermediates in mitosis could account for the observed instability at fragile sites in Pol η–deficient cells. To confirm the persistence of under-replicated DNA in mitosis, we next quantified 53BP1 body formation in G1 daughter cells, hallmark of incomplete DNA replication during the previous cell cycle (Harrigan et al., 2011; Lukas et al., 2011). As already reported (Harrigan et al., 2011; Lukas et al., 2011), we verified that depletion of ATR increases formation of 53BP1 nuclear bodies whereas disruption of SMC2, necessary for the stability of condensed chromatin, reduces the number of 53BP1 nuclear bodies (Fig. S4 B). By following similar experimental procedures, we showed that Pol η–depleted cells and XPV cells displayed an increased number of 53BP1 nuclear bodies in G1 in response to APH treatment compared with their counterpart control cells (Fig. 3 C, Fig. S3, and Fig. S4 A), albeit at a lesser extent compared with ATR depletion. A significant increase in 53BP1 bodies was also observed in unstressed U2OS ShPol η cells, whereas this increase was less significant in XPV cells (Fig. 3 C, Fig. S3, and Fig. S4 A). This could be due to the existence of adaptation pathways in patient-derived cells that completely lack Pol η function, leading to compensatory mechanisms in unstressed conditions. We conclude from these experiments that the absence of Pol η is sufficient to increase the vulnerability of fragile genomic regions, spontaneously or exposed to low level of replication stress, by delaying replication completion at these sequences.

Pol η deficiency induces a checkpoint-blind replication stress

We next reasoned that under-replicated DNA at CFSs persisting into mitosis in the absence of Pol η may result from forks stalled within CFSs that escape the ATR/Chk1 replication checkpoint. We first addressed this issue in Pol η–depleted U2OS cells by monitoring replication protein A (RPA) focus formation, an indicator of endogenous ssDNA accumulation due to fork stalling. Pol η–deficient cells showed higher levels of RPA focus formation (Fig. 4 A, left) and a significant increase in the number of RPA foci per nucleus (Fig. 4 A, middle and right) as compared with control cells containing Pol η, supporting that the absence of Pol η triggers a prolonged fork arrest. However, when we assayed Pol η–depleted cells for Chk1 phosphorylation on serine 345, the main effector of the ATR checkpoint pathway (Zou et al., 2002; Cimprich and Cortez, 2008), we failed to detect a chronic activation of the replication checkpoint (Fig. 4 B). This result suggests that the absence of Pol η is not sufficient to activate the replication checkpoint, despite the increased level of ssDNA. We confirmed the absence of chronic Chk1 phosphorylation in XP30RO cells as compared with their Pol η–complemented counterpart (Fig. 4 C, compare lanes XPV and XPV+WT Pol η). These findings support the hypothesis that loss of Pol η may trigger CFS instability through a mild replicative stress that escapes the replication checkpoint.

The presence of a catalytically inactive Pol η induces a replication stress that strongly activates the replication checkpoint

To further demonstrate that Pol η acts at stalled forks during S phase, and that the catalytic activity is required for its cellular function, we expressed the catalytic inactive form of Pol η (Dead Pol η) in Pol η–deficient cells, and we evaluated the manifestations of replicative stress. We found that expression of the Dead Pol η in XPV cells (two independent stable cell clones were analyzed, XPV+Dead-Polη 1 and XPV+Dead-Polη 2), and not the WT Pol η strongly activated the replication checkpoint revealed by enhanced Chk1 phosphorylation (Fig. 4 C). In agreement with this result, chromatin fractionation followed by immunoblotting showed hyperloading of RPA to chromatin specifically in cells expressing the Dead Pol η (Fig. 4 D), indicative of endogenous

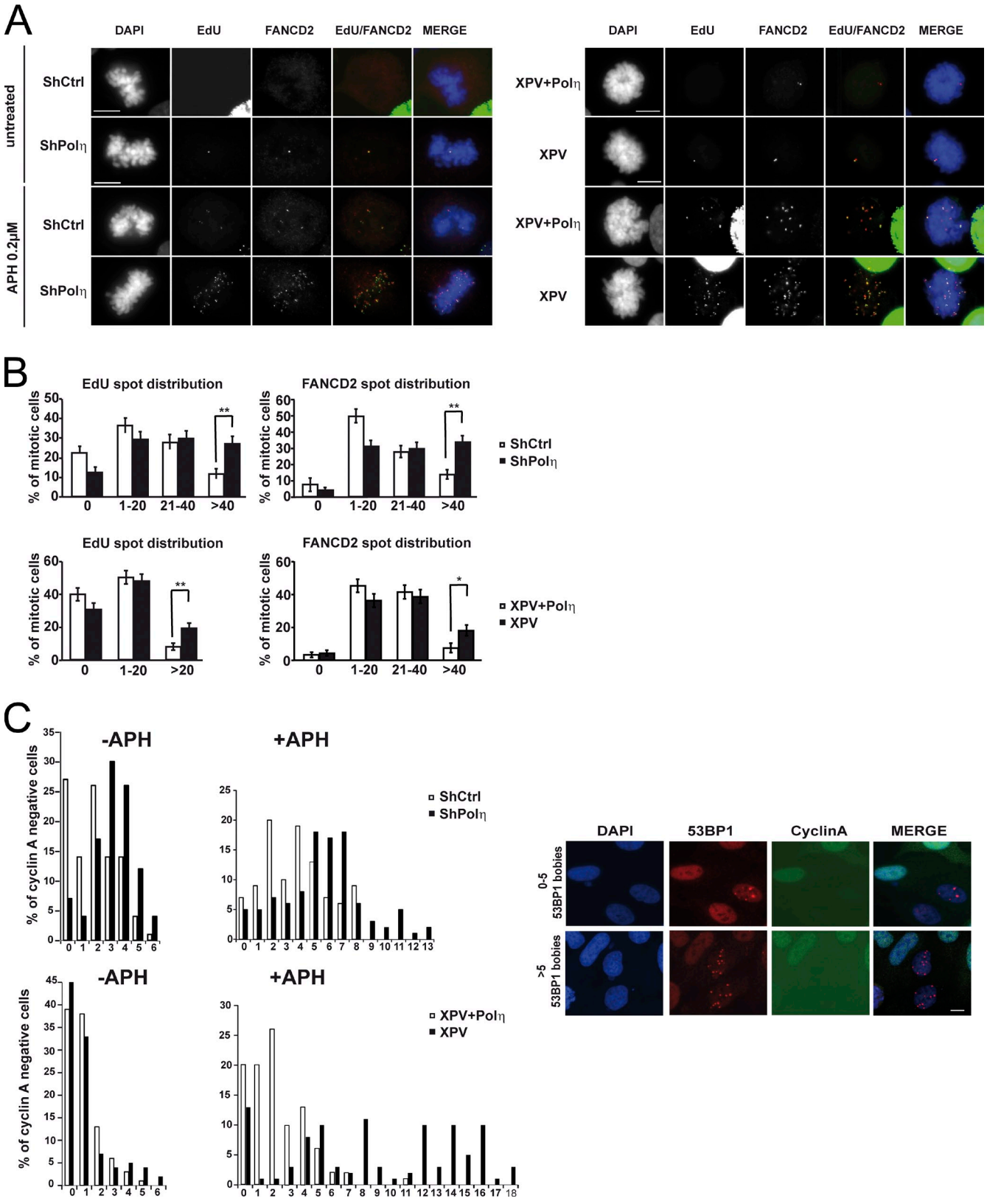

Figure 3. **Pol η deficiency leads to DNA replication delay and persistence of under-replicated regions in mitosis and G1.** (A and B) EdU incorporation and FANCD2 staining in untreated or APH-treated mitotic cells. (A) Representative images of DAPI (grayscale), EdU (grayscale), FANCD2 (grayscale), FANCD2 (red) + EdU (green) merged image, FANCD2 (red) + EdU (green) + DAPI (blue) merged image in mock-depleted and Pol η–depleted U2OS cells (left panels), XP30RO cell and XP30RO cells stably complemented with the WT Pol η (right panels). Bar, 10 μM. (B) Quantification of EdU and FANCD2 spot distribution in the indicated APH-treated mitotic cells as indicated in Materials and methods. The frequency of mitotic cells at prometaphase and metaphase presenting the indicated number of EdU or FANCD2 spots is reported. Error bars represent standard error. *, $P < 0.05$; **, $P < 0.01$ with the χ^2 test. (C) Histograms: quantification of 53BP1 bodies in G1 nuclei from the indicated cell lines, untreated or treated with 0.2 μM APH. Cyclin A–negative cells

ssDNA accumulation due to fork stalling. To further investigate the molecular basis of the recruitment of the Dead Pol η at stalled forks, we repeated the experiments with cells expressing Dead Pol η forms carrying mutations in the ubiquitin-binding domain (UBZ) or in the C-terminal PCNA-interacting protein (PIP) motif, two domains of Pol η critical for its recruitment to chromatin in the TLS process facilitating the bypass of blocking lesions, thereby rescuing DNA replication and preventing fork collapse (Kannouche et al., 2004; Bienko et al., 2005). The UBZ mutation consists of a D-to-A substitution at position 652 (D652A) and the PIP mutation consists of a deletion of the last nine amino acids (ΔPIP; Schmutz et al., 2010). In contrast to the Dead Pol η, we found that the D652A, ΔPIP, and D652A-ΔPIP mutants do not form spontaneous foci when stably expressed in XPV cells, and accordingly we showed that the replication checkpoint was abolished in XPV cells stably expressing these three mutants (Fig. 4 E; Fig. S5 A). Collectively, these data suggest that the catalytically inactive Pol η exerts a dominant-negative effect by being recruited but then being unable to work and that the recruitment of Dead Pol η to stalled forks in unstressed S phase requires both the UBZ and PIP domains, similarly to its enrollment for TLS.

Moreover, we found that all S phase nuclei with Dead Pol η foci are positive for γ-H2AX, an indicator of DNA strand breakage, and all Dead Pol η foci colocalized with γ-H2AX foci (Fig. 5 A), suggesting that the presence of the inactive Pol η induces prolonged fork arrest and collapse. Because homologous recombination (HR)–related processes have a central function in the recovery of stalled or collapsed replication forks (Alabert et al., 2009), we speculated that expression of the Dead Pol η could stimulate the recruitment of HR proteins and induce HR processes. Thus, we performed double immunostaining experiments, and found that indeed Dead Pol η, but not WT Pol η, formed foci that colocalized with the HR RAD51 and BRCA1 proteins (Fig. 5 A). Next, we measured spontaneous sister chromatid exchange (SCE), the cytogenetic consequence of an HR event during DNA replication (Sonoda et al., 1999), whose baseline level directly reflects the integrity of this process (Takata et al., 2001). Comparison of SCEs between control cells and cells expressing WT Pol η revealed no significant difference in the formation of spontaneous SCEs (Fig. 5 B). In contrast, we observed a significant increase in SCEs in cells expressing Dead Pol η (Fig. 5 B). We then assessed CFS instability by using a FISH (fluorescence in situ hybridization)–based assay in order to quantify the fraction of rearrangements (translocations, amplifications, deletions) that localized to the fragile site 7q32.3 (FRA7H) with a FRA7H probe. As shown in Fig. 5 C, we observed a significant twofold increase in FRA7H expression in cells expressing Dead Pol η as compared with control cells and cells expressing a similar level of WT Pol η (Fig. S5 B), supporting that part of replication stress induced by the recruitment of the Dead Pol η arose at CFSs. Finally, we found that expression of the Dead Pol η, and not the WT Pol η, strongly stimulated cell apoptosis, revealed by enhanced proteolytic cleavage of caspase-3 (Fig. S5 C). Taken together, these results suggest that the catalytically inactive Pol η is recruited at CFSs, but because of its higher residence time linked to its inability to synthesize DNA, it impedes access of endogenous Pol η or alternative fork rescue proteins, hence intensifying replication stress, resulting in CFS instability, and exacerbating checkpoint response triggering cell death.

Discussion

Replication forks commonly encounter DNA sequences that are intrinsically difficult to replicate, such as natural pause sites (Tourrière and Pasero, 2007; Branzei and Foiani, 2010). CFSs, relatively large regions of chromosomal DNA that can be replicated in late S phase and are prone to breakage (Durkin and Glover, 2007), may represent endogenous replication barriers within the human genome. CFSs are particularly relevant in cancer development, as recent results from the cancer genome project revealed that a significant fraction of somatic homozygous deletions in human cancer are associated with these fragile genomic regions (Bignell et al., 2010) and CFS rearrangements are observed in the earliest stages of the cancer development (Bartkova et al., 2005; Gorgoulis et al., 2005). Apart from challenging the integrity of replication forks per se, replisome stalling within CFSs may increase the probability of leaving fractions of the genome incompletely replicated or with unresolved replication intermediates, consequently increasing the proportion of cells entering cell division with uncompleted DNA replication. Therefore, replication barriers may represent sequences at risk for structural rearrangements, providing an endogenous source of chromosomal instability.

The known molecular mechanisms affecting CFS stability seem to be focused around two critical aspects of the replication program: the frequency of initiation events in the vicinity of CFSs (Letessier et al., 2011) and the efficiency of replication fork progression (Schwartz et al., 2006; Helmrich et al., 2011). In a chromosomal region with a paucity of active origins, replication forks have to travel through very long distances, increasing the probability of encountering subregions with the potential to form non-B DNA secondary structures (Wang and Vasquez, 2006), which constitute a challenge to fork movement. This is well illustrated by recent data indicating that under conditions of mild replication stress, there are few, if any, new origins to rescue the inherently slow progression of the replication fork (Ozeri-Galai et al., 2011). Thus, chromosomal instability at some fragile sites may result from multiple factors, including the structural complexity of the DNA sequence, the generation of paused or stalled replication forks, and the activation of additional origins of replication under normal physiological conditions.

We provide here unprecedented insights supporting that in unstressed cells or after partial inhibition of the replicative

were scored and classified in the indicated categories based on the number of 53BP1 nuclear bodies. The data shown are from a single representative experiment out of three repeats. For the experiment shown, *n* = 100; example of images of the 53BP1 bodies (red), cyclin A (green), and DAPI (blue) staining from APH-treated Pol η–depleted cells is shown on the right. Images were obtained from a microscope (63× objective, model DMLA; Leica). Bar, 10 µM.

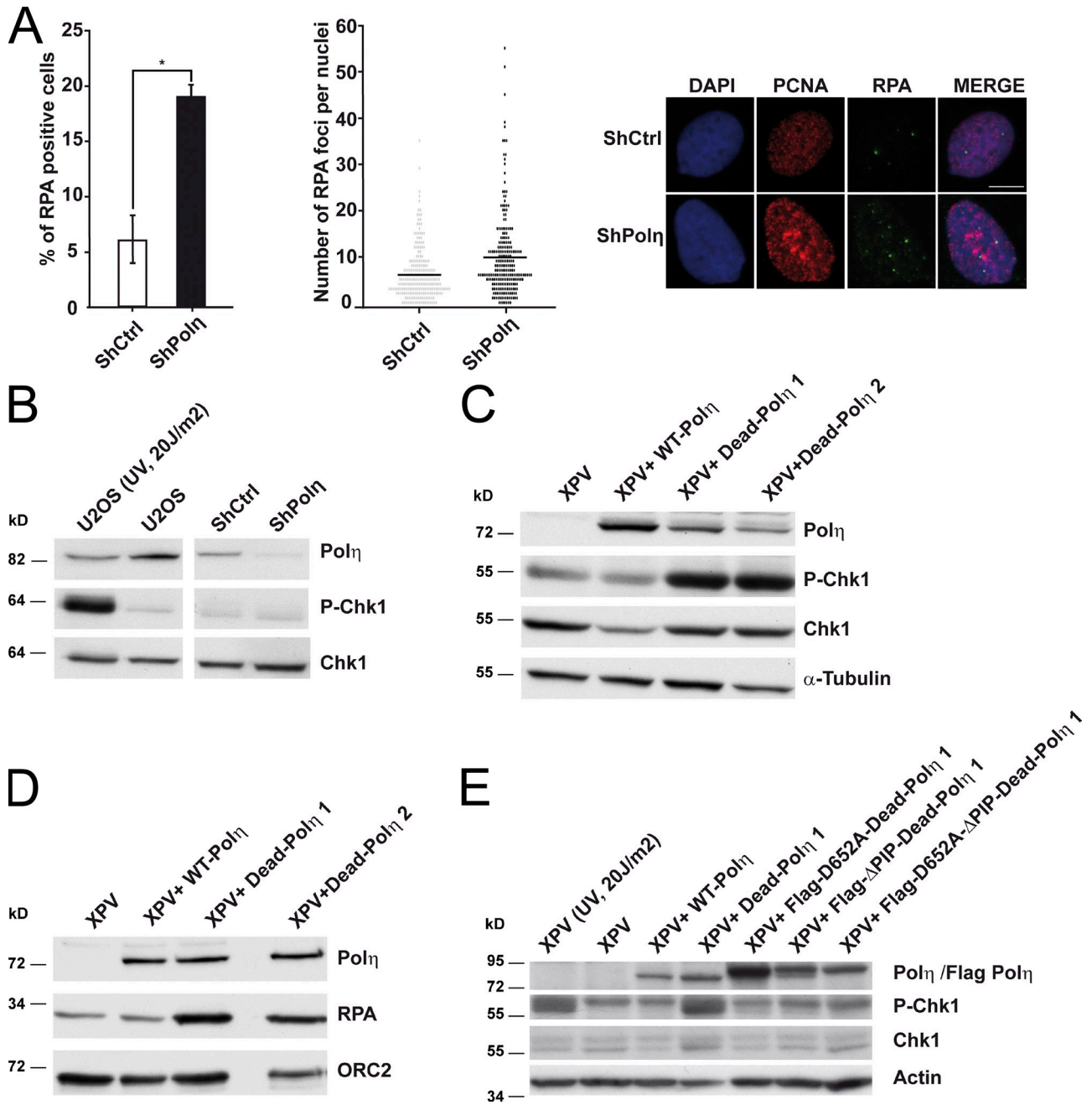

Figure 4. **Analysis of the replication stress in Pol η–deficient cells and Dead Pol η–expressing cells.** (A) Left and middle: mock-depleted (ShCtrl) and Pol η–depleted (ShPolη) U2OS cells were randomly acquired with wide-field microscopy ($n > 70$ cells) in three independent experiments. Quantification of RPA-positive nuclei (right) and number of RPA foci per nucleus (middle) was performed in PCNA foci–positive nuclei (S phase). For the quantification of RPA-positive cells, the p-value was determined with the t-test (*, $P = 0.019$; standard deviations are indicated by error bars. The number of RPA foci per nucleus was counted with ImageJ software ($n = 234$; National Institutes of Health). The p-value was determined with the non-parametric Mann-Whitney test (***, $P < 0.005$). Right: example of images from ShCtrl and ShPolη cells immunostained with anti PCNA (red), anti RPA (green), and DAPI (blue). Triton preextraction was performed before fixation. Bar, 10 µM. (B) Analysis of Chk1 phosphorylation in Pol η–depleted U2OS cells. Anti-Pol η, P-Chk1(ser 345), and Chk1 immunodetection on whole extracts from U2OS cells treated with UV (20J/m^2, 6 h) as positive control for Chk1 phosphorylation, U2OS cells untreated and U2OS cells mock depleted (ShCtrl), or Pol η–depleted (ShPolη). Chk1 serves here as a loading control. (C) Extracts from XPV cells, XPV cells stably complemented with Pol η WT (XPV+Polη WT), or the Dead form of Pol η (XPV+Polη Dead1 and XPV+Polη Dead2) were fractionated and the soluble fractions were analyzed by immunoblotting for the detection of Pol η, P-Chk1(ser 345), Chk1, and α-tubulin as loading control. (D) The chromatin fraction from extracts described in C were analyzed by immunoblotting for RPA level into the chromatin. ORC2 was used as a loading and fractionation control. (E) Requirement of PIP and UBZ domains of Dead Pol η for its ability to activate the replication checkpoint. Extracts from XPV cells, XPV cells stably complemented with wild-type Pol η (XPV+WT Polη), Dead Pol η (XPV+Dead Pol η), D652A-Dead Pol η (XPV+Flag-D652A-Dead Pol η), ΔPIP-Dead Pol η (XPV+Flag-ΔPIP-Dead Pol η), or the double mutant D652A-ΔPIP Dead Pol η (XPV+Flag-D652A-ΔPIP-Dead Pol η) were analyzed by immunoblotting for the detection of Pol η, P-Chk1(ser 345), Chk1, and actin as loading control. The detection of Pol η was performed with Pol η antibodies (Abcam) in extracts from XPV+WT Polη, XPV+Dead Pol η, and XPV+Flag-D652A-Dead Pol η while the XPV+Flag-ΔPIP-Dead Pol η and the XPV+Flag-D652A-ΔPIP-Dead extracts were blotted with the FlagM2 antibody because the ΔPIP mutants are not recognized by the Pol η antibody (Abcam). Extracts from XPV cells treated with UV (20J/m^2, 6 h) serves as positive control for Chk1 phosphorylation.

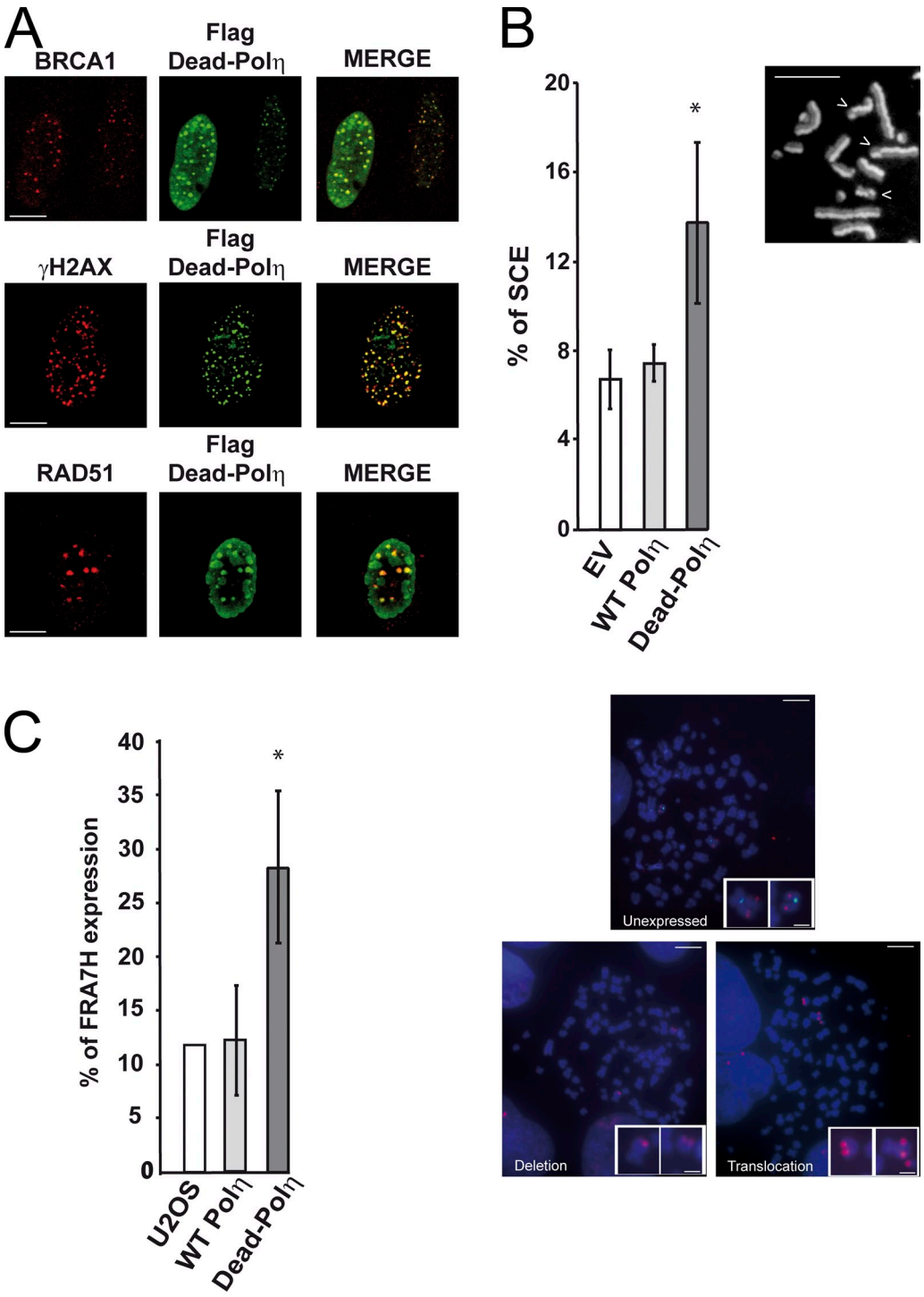

Figure 5. **Expression of Dead Pol η stimulates homologous recombination and results in CFS instability.** (A) Pol η (green), γH2AX (red), BRCA1 (red), and Rad51 (red) foci formation were revealed by immunofluorescence in U2OS cells transiently transfected with pcDNA-Flag-Dead Pol η. Triton preextraction was performed before fixation. Images obtained from confocal analysis show the colocalization of each protein with Dead Pol η. Bars, 10 μM. (B) Sister chromatid exchange analyses in U2OS cells transiently transfected with pcDNA (empty vector), pCDNA-Flag-WT Pol η, or pcDNA-Flag-Dead Pol η cells were labeled with BrdU for 45 h and treated with Karyomax for 3 h. Metaphases were spread on a glass slide and stained with Hoechst as described in Materials and methods. Differential incorporation of BrdU in each chromatid is obtained after DAPI staining and sister chromatid exchange (noted with arrows; bar, 10 μM) is scored (>3,000 chromosomes, 3 independent experiments). Standard deviations are indicated by error bars. The statistical significance was assessed using *t* test; *, P = 0.042. (C) Quantification and illustration of the expression of the common fragile site FRA7H (translocations, amplifications, deletions) analyzed by FISH in WT and Dead Pol η–expressing U2OS cells (3 experiments; $n > 20$ metaphases; standard deviations are indicated by error bars). The statistical significance was assessed using *t* test; *, P = 0.017. Red, FRA7H probe; green, chromosome 7 centromeric probe. Bar, 10 μM (2 μM, insets).

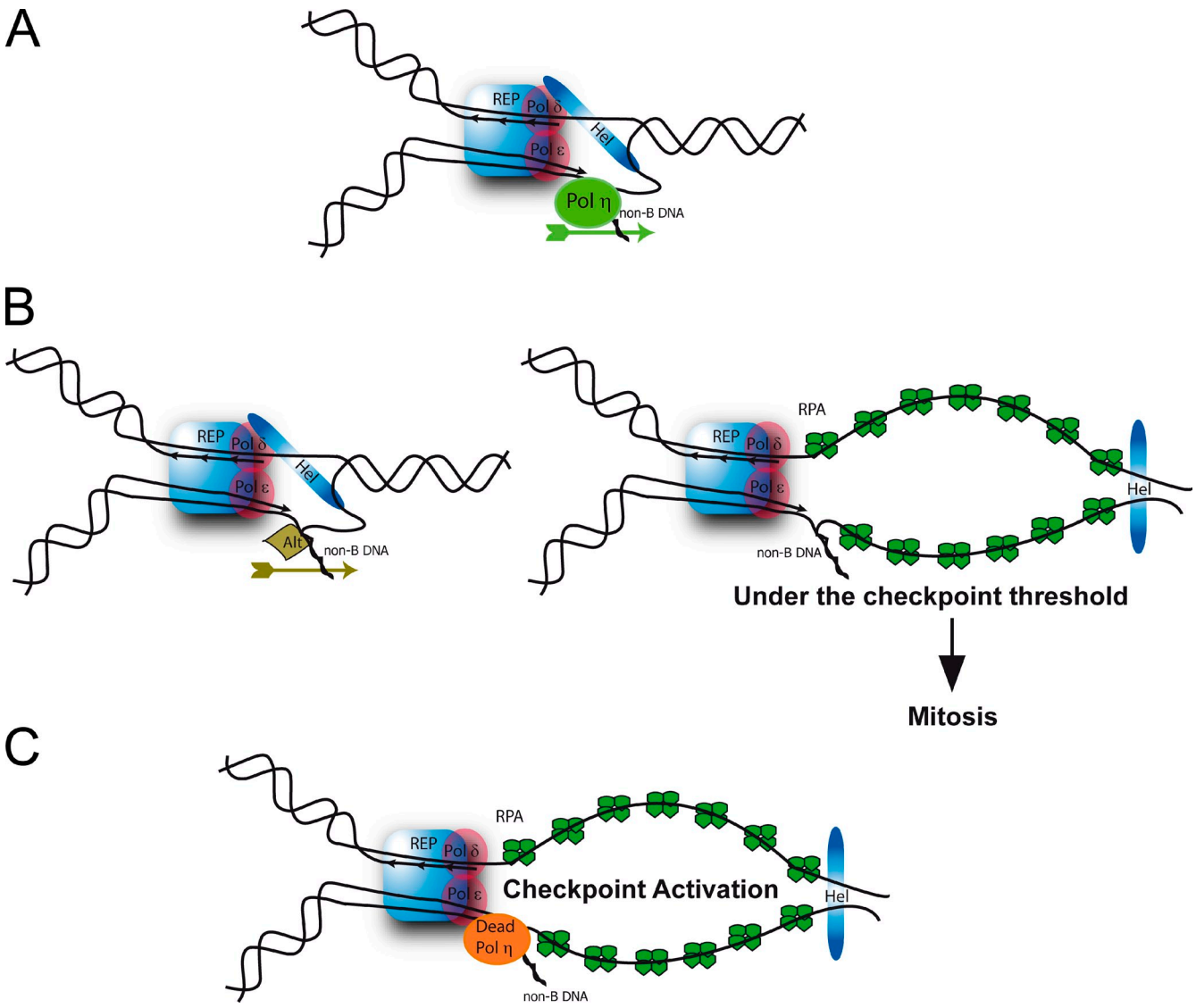

Figure 6. **A model for the role of Pol η at stalled forks within CFS.** In particular structured DNA containing subregions of CFSs that impede fork progression, slowdown or arrest of the replicative DNA polymerases causes partial functional uncoupling of the MCM helicase and the stalled replicative DNA polymerase activities, resulting in production of short stretches of ssDNA. In DNA sequences able to adopt stable secondary structures, intramolecular folding could be formed. (A) In wild-type cells, Pol η is recruited and can perform DNA synthesis through these structures, preventing unresolved replication intermediates. (B) In the absence of Pol η, this DNA synthesis through non-B DNA can be partially rescued by alternative factors (left), but a subpopulation of stalled forks escape to this rescue pathway, generating under-replicated ssDNA after further uncoupling between polymerases and helicases in a checkpoint-blind manner, which persists into mitosis (right). (C) In the presence of inactive Dead Pol η, no DNA synthesis through structured DNA is possible by endogenous Pol η or alternative factors, causing persistent fork stalling, increased uncoupling, ssDNA accumulation, and activation of the replication checkpoint or fork collapse.

DNA polymerases, Pol η is recruited to stalled forks within CFSs and efficiently synthesizes DNA through non-B DNA structures, thus preventing under-replicated CFS DNA in mitosis.

We propose the following model to explain our results, based on the assumption that specific CFS subregions may impede replication fork progression (Fig. 6). Such subregions can include DNA sequence contexts that compromise processive synthesis by replicative polymerases such as Pol δ (Fig. 2). Pausing of replicative DNA polymerases or unequal rates of leading/lagging strand synthesis may cause partial uncoupling of the replicative helicase and polymerase activities, resulting in the production of ssDNA tracts. In DNA sequences able to adopt stable non-B DNA secondary structures, the intramolecular folding into non-B structures is expected to be favored in the absence of competition from the complementary strand. The resulting structured DNA may then act as further structural impediments to the replicative DNA polymerases. As a consequence, Pol η may be required for efficient synthesis through these structures to avoid incompletely replicated regions or unresolved replication intermediates. We provide evidence that the recruitment of Pol η in this process requires both the UBZ and PIP domains, similarly to its enrollment for TLS (Fig. 4 E).

We discovered that the low replication stress induced by the absence of Pol η escapes the replication checkpoint; in contrast, the checkpoint is over-activated when the Dead Pol η is expressed. Our interpretation of these results is that Pol η could

function at the fork as part of the replisome and that an alternative pathway can perform DNA synthesis at structured DNA within CFSs in the absence of Pol η, whose accessibility is inhibited in the presence of Dead Pol η. This subtle and more focused role of Pol η could explain why the effect of Pol η depletion is mild compared with ATR deficiency, which leads to a major global checkpoint defect.

The efficiency of Pol η synthesis through structured DNA may be explained by specific structural features of the polymerase itself. Indeed, a recent study showed that interfacial residues of the back of the little finger subdomain of Pol η interact with a neighboring DNA molecule (Biertümpfel et al., 2010). The authors of this study suggest that the back of the little finger of Pol η may be a downstream DNA-binding site, and the little finger subdomain of Pol η may serve as a wedge to separate non-B form DNAs, and aid the molecular splint to complete replication through structured DNA. It would be interesting in the future to evaluate the importance of these interfacial residues for the Pol η function at CFSs.

Why should the cell use an error-prone DNA polymerase to carry out specialized DNA synthesis that is necessary to maintain genomic stability? Possibly, Pol η synthesis is restricted to a very short stretch of CFS sequence. The decreased accuracy of Pol η for base substitution errors may be a price worth paying in order for the cell to complete fork progression through structured DNA, avoiding fork stalling and DNA breakage, which is potentially more detrimental to genome integrity.

In conclusion, the cell lifespan depends on a subtle equilibrium between accurate genomic DNA synthesis, necessary for duplication of the genotype before chromosomal partitioning during mitosis, and less stringent DNA transactions involving the TLS DNA polymerases, necessary for cells to tolerate not only exogenous insults, but also endogenous structural DNA perturbations, which could be a necessary "flexibility" process.

Materials and methods

Cell culture and treatments

U2OS cell line (American Type Culture Collection) was cultured in DMEM (Gibco) supplemented with 10% FBS (Lonza), penicillin, and streptomycin. 150 µg/ml hygromycin B was added to the medium for mock-depleted, Pol η-depleted U2OS cells, and U2OS cells stably expressing Flag-Pol eta WT or Flag Pol eta Dead. XP30RO cells (from a patient who carries a POLH gene deletion that leads to truncation of Pol η at residue 35) were grown in α-MEM medium (Gibco) supplemented with 10% FBS (Lonza), penicillin, and streptomycin. Stable clones expressing WT or Dead Pol eta in XP30RO cells were maintained in α-MEM medium containing 100 µg/ml zeocin (InvivoGen). Cells were grown in a 5% CO_2, 37°C incubator. Transient expression of WT or Dead Pol η was obtained 48 h after (pcDNA 3.1 Flag-Pol eta WT or pcDNA 3.1 Flag-Pol eta Dead) vector transfection using JetPEI (Polyplus Transfection). 0.2 µM Aphidicolin (Sigma-Aldrich) was added to the culture medium for 24 h, as indicated. The siRNAs used were: ATR: Ambion Silencer-Select (siRNA ID s536), sense sequence (5′-UUGUAGAAAUGGAUACUGA-3′). SMC2: Ambion Silencer-Select (siRNA ID s20794), sense sequence (5′-CUAUCACUCUGGACCUGGA-3′). SiCTRL (against luciferase; Sigma-Aldrich) 5′-CGUACGCGGAAUACUUCGA-3′. 50-nM siRNA duplexes were transfected into U2OS cells using Lipofectamine 2000 (Invitrogen).

Generation of mutant Pol η

D652A, ΔPIP (deletion generated by introducing a stop codon at position 705 promoting a deletion of the last nine amino acids of the Polη protein), and the double mutant D652A-ΔPIP mutations were generated in pCDNA 3.1/Hygro Flag-Dead Pol η (Rey et al., 2009). XP30RO cells were stably transfected with the different constructs (JetPEI; Polyplus Transfection) and selected in the presence of 150 µg/ml hygromycin (Invitrogen).

Chromatin immunoprecipitation (ChIP)

Formaldehyde was added to the culture medium to a final concentration of 1% and cross-linking was allowed to proceed for 15 min at room temperature. To stop the reaction, glycine was added to a final concentration of 0.125 M for 10 min. Cells were washed with PBS, harvested by scraping before being lysed in the buffer: 5 mM Pipes, pH 8, 85 mM KCl, and 0.5% NP-40. Nuclei were then incubated in nuclear lysis buffer (50 mM Tris-HCl, pH 8.1, 10 mM EDTA, and 1% SDS) and chromatin was sonicated (Branson Sonifier 250) to obtain DNA fragments of ∼500–1,000 bp. Diluted samples were then subjected to a 1-h preclearing with blocked protein A and protein G beads (Sigma-Aldrich). For each condition, 200 µg of the precleared samples were immunoprecipitated overnight at 4°C using 2 µg of rabbit polyclonal anti-Pol η (ab17725; Abcam), and 2 µg of rabbit polyclonal anti IgG as negative control (mock; Cell Signaling Technology). Immune complexes were then recovered by incubating the samples with blocked protein A/protein G beads for 2 h at 4°C. Beads were washed once in dialysis buffer (2 mM EDTA, 50 mM Tris-HCl, pH 8, and 0.2% Sarkosyl), five times in wash buffer (100 mM Tris-HCl, pH 8.8, 500 mM LiCl, 1% NP-40, 1% NaDoc). The bead/chromatin complexes were resuspended in 200 µl of TE buffer (10 mM Tris-HCl, pH 8, and 0.5 mM EDTA, pH 8). Cross-link was reversed by adding 0.5% SDS and RNase A to the samples and incubating overnight at 70°C. After a 2-h proteinase K treatment, DNA was purified with phenol/chloroform and precipitated. ChIPs were analyzed by real-time qPCR using primers proximal to several breakpoint sites within CFSs and to nonfragile regions within GAPDH and DHFR. Primer sequences are as follows: DHFR, sense 5′-GCCATCCTTCAACGCAATAAGTACG-3′, anti-sense 5′-GAATTCATGAAAACGTAGCTCGTCC-3′; GAPDH: sense 5′-CCCTCTGGTGGTGGCCCCTT-3′, anti-sense 5′-GGCGCCCAGACACCCAATCC-3′; FRA7H.1: sense 5′-TAATGCGTCCCCTTGTGACT-3′, anti-sense 5′-GGCAGATTTTAGTCCCTCAGC-3′; FRA7H.2: sense 5′-TGAGCCATTCTGTCACCAAG-3′, anti-sense 5′-AACCTTCCTACTGCCTGCTG-3′; FRA16D: sense 5′-TCCTGTGGAAGGGATATTTA-3′, anti-sense 5′-CCCCTCATATTCTGCTTCTA-3′; FRA3B: sense 5′-TGTTGGAATGTTAACTCTATCCCAT-3′, anti-sense 5′-CATATCTCATCAAGACCGCTGC-3′.

In vitro primer extension assay on CFS sequences

Recombinant human four-subunit polymerase δ was expressed in Sf9 insect cells using a baculovirus vector containing POLD1, 2, 3, and 4 genes, and purified by fast protein liquid chromatography (Xie et al., 2002). Human polymerase η was purchased from Enzymax. FRA16D and FRA3B sequences were obtained from GenBank accession nos. AF217490 and 183583557. Sequences predicted to form non-B DNA structures were identified within the reference sequences for FRA16D and FRA3B using the non-B DNA database (http://nonb.abcc.ncifcrf.gov). Oligonucleotides corresponding to CFS sequences were converted to double-stranded fragments using T7 DNA polymerase and cloned into the BamH1 site of the pGEM3Zf(−) vector (Promega; Shah et al., 2010). To produce single-stranded DNA templates, F′ *Escherichia coli* carrying the pGEM vectors were infected with R408 helper phage, and single-stranded DNA was purified from phage particles by phenol-chloroform extraction. Primer extension reactions were performed with 100 fmol primed, single-stranded DNA and excess DNA polymerase, ranging from 500 fmol to 1 pmol. Amounts of Pols δ and η used in primer extension reactions were determined by titration on the control CFS template, in order to achieve 80–85% transit past the CFS region by reaction completion (15-min time point) and to ensure that percent transit was similar between the two polymerases at each time point (to control for differences in polymerase activity). The standard reaction buffer for both polymerases was identical, and contained 25 mM KPO_4, pH 7.6, 5 mM $MgCl_2$, 2.5 mM DTT, 0.2 mg/ml nonacetylated BSA, and 250 µM dNTPs. DNA template and buffer were preincubated at 37°C for 3 min and reactions initiated by addition of polymerase. Reactions were terminated by addition of an equal volume of stop dye at indicated time points. For quantification, the percent transit was calculated as [(number of products in 3′ region)/(number of products in CFS + 3′ region)], and the normalized percent transit was calculated as: (percent transit on the template of interest/percent transit on the control template). Statistical significance was determined by *t* test analysis.

Sequences predicted to form non-B DNA structures within FRA16D and FRA3B sequences

The location of each sequence within the reference genome is given in parentheses. Control CFS template (FRA16D, 199256–199392):

5′-AAAACTTCTGGTTTAACAAGGTAGACCTTTTTAAATTCGTTGTTTTATTTGTTTCATCATATCCTGAATATTGTATTTCGTATTTTATTTACAGGTACTCACATGGCACTATCTTTATTTACTAATTTATTTATTTACGTACGGCGTTGCGC-3′; FRA16D template 1 (191565–191712): 5′-AGAGTACAGAGTCGGAGGGTTCATCGACCCTGATGTTCCCGTCCGGGGGTACGTACCGATGTATATATATATATATATATATATATATATATATATATATATAAATATATATGAAAAAAAAAAAAAAAAAAAAAAAAAAAAAATCATCTTTA-3′; FRA16D template 2 (191713–191860): 5′-GATATACACCTGGAGTGTGTGCCCTTTTCTACTTGCATTACACTTTTTTTTTTTTTTTTTTTTGAGATGGCGTCTTGCTCTGTTGCCCAGGCTGGAGTGCAGTGGCGATCTCAGCTTACTGCAACCTCCGACTCCCAGGTTCAAGCGAT-3′, FRA3B template (837821–837929; 837963–838030): 5′-TTTTTTTTTTTTTTTTTTTTTCAACCCTCCCAATTAATCAACTGAAAGTCAATTGACATCCTTCTCAATCCAAGTTATGGTAAATTCTTTTCGTTCTTTTTATACATATGTGCATATATATATATATATATATATATATATATATATATATATATATATATATATGTGTGT-3′. The potential for the insert sequences to form thermodynamically stable hairpin structures was determined by Mfold analysis (http://mfold.rna.albany.edu/?q=mfold).

FRA16D template 1 contains a mononucleotide [A]28 repeat with the potential to form bent DNA (Koo et al., 1986; Strahs and Schlick, 2000) and slipped strands, and an interrupted [TA]24 repeat predicted to form a hairpin structure. FRA16D template 2 contains a [T]19 repeat capable of forming bent DNA and slipped strands, and an interrupted inverted repeat (IR) of 36 bases predicted to form a stable hairpin structure. The FRA3B template contains a [T]22 repeat capable of forming bent DNA and slipped strands, and a [TA]25 repeat predicted to form a hairpin structure. Finally, the control CFS template is AT rich (75%), but does not contain any repeat structures with non-B DNA structure potential.

Polymerase η fidelity assay

Polymerase η reactions were performed as described above using 2 pmol unlabeled, G40-primed, single-stranded FRA16D template 2 and 20 pmol human Pol η. Reactions were incubated for 60 min at 37°C. Products were restriction digested with BamHI, agarose gel purified, ligated into the pGem3zf(−) vector, and transformed into DH5α *E. coli*. Plasmid DNA was isolated from random clones, and the sequences determined using the M13R primer. Reactions with human four-subunit polymerase δ were performed using two reaction conditions: standard reaction conditions, using 1 pmol template DNA, 5 pmol PCNA, and 10 pmol polymerase δ; and reaction conditions established for RFC loading of PCNA, using 1 pmol DNA template, 0.5 pmol RFC, 4 pmol PCNA, and 3 pmol polymerase δ. Reaction products were cloned and sequenced as for Pol η reactions. For comparison, control reactions were also performed with 5 U exonuclease-deficient Klenow (USB) and 1 pmol DNA template, and clones were sequenced as above.

CFS-delayed replication experiments using EdU incorporation

CFS-delayed replication was examined using an in situ 5-ethynyl-2′-deoxyuridine (EdU) incorporation assay. Cells grown on glass coverslips were left untreated or treated with 0.2 µM APH for 24 h and labeled with 10 µM EdU for 45 min before fixation. Cells were fixed in PBS containing 4% paraformaldehyde for 15 min and then permeabilized in PBS/0.5% Triton X-100 for 20 min. EdU was detected by click reaction using the Click-iT EdU Imaging kit (Invitrogen), according to the manufacturer's instructions. Images were acquired at 20°C in Vectashield mounting medium (Vector Laboratories) using a microscope (Axio Imager Z1; Carl Zeiss) with a Plan Apochromat 63×/1.4 NA objective, equipped with an Orca-ER CCD camera (Hamamatsu Photonics). A series of 0.24-µm Z-stack images was collected and orthogonal projections were reconstituted using the Axiocam software.

Immunofluorescence and microscopy

Cells were grown on glass coverslips and fixed with 4% paraformaldehyde (PFA) for 15 min at RT followed by incubation with 0.5% Triton X-100 in PBS for 10 min at RT or preextracted for 5 min in CSK (10 mM Pipes, pH 7.5, 100 mM NaCl, 300 mM sucrose, 3 mM $MgCl_2$, and 1× HaltTM protease/phosphatase inhibitors [Thermo Fisher Scientific]) with 0.5% Triton X-100 before PFA fixation. After fixation cells were washed in PBS and blocked with 5% goat serum (Sigma-Aldrich) in PBS. Cells were incubated with primary antibodies (1 h at RT) in PBS, washed with PBS, and then incubated with Alexa Fluor 488 or 555 goat anti–mouse or anti–rabbit (1:1,000; Molecular Probes) for 1 h at RT in PBS. DNA was counterstained with DAPI in Vectashield mounting agent (Vector Laboratories). Rabbit polyclonal antibodies were as follows: Pol η (1:200, ab 17725; Abcam), PCNA (1 µg/ml, ab 18197; Abcam), phospho-histone H2AX (ser138, 1:50, 2577; Cell Signaling Technology), Rad51 (1:500, P1C130; EMD Millipore), 53BP1 (1:200, ab21083; Abcam), FANCD2 (ab2187; Abcam), and phospho-histone H3 (ser10; EMD Millipore). Mouse monoclonal antibodies were as follows: anti-FLAG M2 (1:100; Sigma-Aldrich), anti BRCA1 (1:100, D-9; Santa Cruz Biotechnology, Inc.), and RPA (1 µg/ml, Ab-2; EMD Millipore). Image acquisition of multiple random fields were performed at 20°C on a wide-field microscope (63×, type PL, NA 1.25; or 20×, type HC PL, NA 0.5 objectives; model DMLA, Leica), using a CCD camera (Cool-Snap HQ; Photometrics) driven by PM Capture Pro 6.0 (Photometrics). For confocal images, cells were analyzed at 20°C on a microscope (100×, type HCX PL APO, NA. 1.4 with the TCSNTV acquisition software; model SP2, Leica).

Cell extracts and immunoblotting

For whole-cell extracts, cells were lysed (50 mM Tris-HCl, pH 7.5, 300 mM NaCl, 1% Triton X-100, 5 mM EDTA, and 1 mM DTT supplemented with Halt protease and phosphatase inhibitors 1× [Thermo Fisher Scientific]) for 30 min at 4°C and sonicated. Chromatin fractionation was performed as in Zou et al. (2002) with the following modifications: solution A (10 mM Pipes, pH 7, 300 mM sucrose, 3 mM $MgCl_2$, 150 mM NaCl, 1 mM EGTA, 1 mM DTT, 0.1%, Triton X-100, 0.5 µg/ml pepstatine, and 1× to 3× HaltTM protease/phosphatase inhibitors [Thermo Fisher Scientific]) was used. Whole-cell extracts and fractionated extracts were boiled in loading buffer (250 mM Tris-HCl, pH 6.8, 5% SDS, 30% glycerol, 20% β-mercaptoethanol, and bromophenol blue). Proteins were separated on 8 or 10% SDS-PAGE gel and electro-transferred (Bio-Rad Laboratories) on PVDF membranes (GE Healthcare). Blots were detected by ECL Western Blotting Substrate (Perbio Science). We used primary antibodies against Pol η (Abcam), FlagM2 (Sigma-Aldrich), phosphorylated Ser 345-Chk1 (Cell Signaling Technology), Chk1 (Santa Cruz Biotechnology, Inc.), PCNA (Abcam), RPA (EMD Millipore), ORC2 (MBL), FANCD2 (Santa Cruz Biotechnology, Inc.), α-tubulin (Sigma-Aldrich), actin (EMD Millipore), vinculin (Abcam), caspase-3 (Cell Signaling Technology), ATR (Cell Signaling Technology), SMC2 (Abcam), and MCM7 (Santa Cruz Biotechnology, Inc.).

Sister chromatid exchange (SCE)

Cells were treated with BrdU at 10 µg/ml for two cell generations (45 h). Cell accumulation in metaphase was induced with karioMax-Colcemid (Gibco) treatment at 10 µM for 3 h. Cells were collected and incubated in hypotonic buffer (50 mM KCl) for 10 min at 37°C. Cells were fixed in cold methanol/acetic acid (3:1) and spread on a glass slide. Slides were incubated in the dark with 12.5 µg/ml Hoechst 33258 for 20 min, followed by ultraviolet exposure (312 nm) for 2 h in the presence of 2× SSC and then incubated in 2× SCC at 60°C for 20 min. Slides were washed and stained with DAPI before mounting in Vectashield medium (Vector Laboratories). Image acquisition of multiple random fields was performed at 20°C on a wide-field microscope (100× objective, 0.5–1.3 oil iris; Eclipse TE300, Nikon), using a digital camera (DXM1200; Nikon) driven by ACT1 software (Nikon).

FISH analysis

Cells were treated with 0.1 µg/ml colcemid (Gibco) for 3 h. Cell pellets were resuspended in hypotonic solution (0.05 M KCl) and incubated for 15 min at 37°C. Cells were then fixed in a methanol/acetic acid solution (3:1). Cell suspension was dropped on slides to obtain spread chromosomes. The BAC 36B6 (RP-11) probe (FRA7H locus) was labeled with the BioPrime DNA Labeling System kit (Invitrogen), purified using the PCR purification kit (QIAGEN), and ethanol precipitated with 0.1 µg/µl human Cot-1 DNA (Invitrogen) overnight at −20°C. Precipitated DNA was incubated for 1 h at 37°C in hybridization mix. Metaphase slides were incubated with Rnase (10 µg/ml in 2× SSC) for 1 h at 37°C followed by dehydration in a successive ethanol bath (70, 85, and 100%). The probe was applied on metaphases, denatured for 8 min at 70°C and hybridized over night at 37°C. Indirect labeling of the probe was obtained by successive layers of Alexa Fluor 555–conjugated streptavidin (Molecular Probes), biotin-conjugated anti-streptavidin (Rockland), and Alexa Fluor 555–conjugated streptavidin. A human green-labeled chromosome 7–specific centromeric probe was also used according to the supplier's recommendations (Abbot Molecular). Image acquisition of multiple random fields was performed at 20°C in Vectashield mounting medium (Vector Laboratories) on a wide-field microscope (63× objectives, type: PL, NA 1.25; model DMLA, Leica), using a CCD camera (Cool-Snap HQ; Photometrics) driven by PM Capture Pro 6.0 (Photometrics).

Online supplemental material

Fig. S1 shows that Dead Pol η is also recruited on FRA3B CFS (A), the effect of replication accessory factors on Polδ synthesis (B and C), and the fidelity of Pol δ and Pol η through FRA16D template (D–F). Fig. S2 demonstrates

that EdU incorporation was observed in mitotic cells (A) and that Pol η depletion doesn't influence FANCD2 monoubiquitination after APH treatment (B). Fig. S3 shows large field microscopy images of 53BP1 and Cyclin A labeling in the different cell lines and conditions. Fig. S4 contains a replica of Fig. 3 C and shows the effect of ATR and SMC2 depletion on 53BP1 body formation in G1 U2OS cells. Fig. S5 shows an additional experiment of Fig. 5 E with independent cellular clones (A), microscopy images of Pol η labeling in cells used for FISH experiment (B), and apoptosis induction after Dead Pol η expression (C). Online supplemental material is available at http://www.jcb.org/cgi/content/full/jcb.201207066/DC1. Additional data are available in the JCB DataViewer at http://dx.doi.org/10.1083/jcb.201207066.dv.

We thank E. Despras and P. Kannouche for XPV cells stably expressing WT-Pol η and Dead Pol η.

This work was supported by La Ligue contre le cancer (Labelisation Program) to J.-S. Hoffmann and F. Rosselli, and an INCa Grant (YPOL-2010) to J.-S. Hoffmann. The project from K.A. Eckert's laboratory was funded, in part, under a grant (SAP4100042746 to K.A. Eckert) with the Pennsylvania Department of Health using Tobacco Settlement Funds. The Department specifically disclaims responsibility for any analyses, interpretations, or conclusions.

The authors declare no competing financial interests.

Submitted: 10 July 2012
Accepted: 27 March 2013

References

Alabert, C., J.N. Bianco, and P. Pasero. 2009. Differential regulation of homologous recombination at DNA breaks and replication forks by the Mrc1 branch of the S-phase checkpoint. *EMBO J.* 28:1131–1141. http://dx.doi.org/10.1038/emboj.2009.75

Bartkova, J., Z. Horejsí, K. Koed, A. Krämer, F. Tort, K. Zieger, P. Guldberg, M. Sehested, J.M. Nesland, C. Lukas, et al. 2005. DNA damage response as a candidate anti-cancer barrier in early human tumorigenesis. *Nature*. 434:864–870. http://dx.doi.org/10.1038/nature03482

Bienko, M., C.M. Green, N. Crosetto, F. Rudolf, G. Zapart, B. Coull, P. Kannouche, G. Wider, M. Peter, A.R. Lehmann, et al. 2005. Ubiquitin-binding domains in Y-family polymerases regulate translesion synthesis. *Science*. 310:1821–1824. http://dx.doi.org/10.1126/science.1120615

Biertümpfel, C., Y. Zhao, Y. Kondo, S. Ramón-Maiques, M. Gregory, J.Y. Lee, C. Masutani, A.R. Lehmann, F. Hanaoka, and W. Yang. 2010. Structure and mechanism of human DNA polymerase eta. *Nature*. 465:1044–1048. http://dx.doi.org/10.1038/nature09196

Bignell, G.R., C.D. Greenman, H. Davies, A.P. Butler, S. Edkins, J.M. Andrews, G. Buck, L. Chen, D. Beare, C. Latimer, et al. 2010. Signatures of mutation and selection in the cancer genome. *Nature*. 463:893–898. http://dx.doi.org/10.1038/nature08768

Branzei, D., and M. Foiani. 2010. Maintaining genome stability at the replication fork. *Nat. Rev. Mol. Cell Biol.* 11:208–219. http://dx.doi.org/10.1038/nrm2852

Casper, A.M., P. Nghiem, M.F. Arlt, and T.W. Glover. 2002. ATR regulates fragile site stability. *Cell*. 111:779–789. http://dx.doi.org/10.1016/S0092-8674(02)01113-3

Chan, K.L., T. Palmai-Pallag, S. Ying, and I.D. Hickson. 2009. Replication stress induces sister-chromatid bridging at fragile site loci in mitosis. *Nat. Cell Biol.* 11:753–760. http://dx.doi.org/10.1038/ncb1882

Cimprich, K.A., and D. Cortez. 2008. ATR: an essential regulator of genome integrity. *Nat. Rev. Mol. Cell Biol.* 9:616–627. http://dx.doi.org/10.1038/nrm2450

Dayn, A., S. Malkhosyan, D. Duzhy, V. Lyamichev, Y. Panchenko, and S. Mirkin. 1991. Formation of (dA-dT)n cruciforms in Escherichia coli cells under different environmental conditions. *J. Bacteriol.* 173:2658–2664.

Debatisse, M., B. Le Tallec, A. Letessier, B. Dutrillaux, and O. Brison. 2012. Common fragile sites: mechanisms of instability revisited. *Trends Genet.* 28:22–32. http://dx.doi.org/10.1016/j.tig.2011.10.003

Durkin, S.G., and T.W. Glover. 2007. Chromosome fragile sites. *Annu. Rev. Genet.* 41:169–192. http://dx.doi.org/10.1146/annurev.genet.41.042007.165900

Durkin, S.G., M.F. Arlt, N.G. Howlett, and T.W. Glover. 2006. Depletion of CHK1, but not CHK2, induces chromosomal instability and breaks at common fragile sites. *Oncogene*. 25:4381–4388. http://dx.doi.org/10.1038/sj.onc.1209466

Fungtammasan, A., E. Walsh, F. Chiaromonte, K.A. Eckert, and K.D. Makova. 2012. A genome-wide analysis of common fragile sites: what features determine chromosomal instability in the human genome? *Genome Res.* 22:993–1005. http://dx.doi.org/10.1101/gr.134395.111

Gorgoulis, V.G., L.V. Vassiliou, P. Karakaidos, P. Zacharatos, A. Kotsinas, T. Liloglou, M. Venere, R.A. Ditullio Jr., N.G. Kastrinakis, B. Levy, et al. 2005. Activation of the DNA damage checkpoint and genomic instability in human precancerous lesions. *Nature*. 434:907–913. http://dx.doi.org/10.1038/nature03485

Harrigan, J.A., R. Belotserkovskaya, J. Coates, D.S. Dimitrova, S.E. Polo, C.R. Bradshaw, P. Fraser, and S.P. Jackson. 2011. Replication stress induces 53BP1-containing OPT domains in G1 cells. *J. Cell Biol.* 193:97–108. http://dx.doi.org/10.1083/jcb.201011083

Helmrich, A., M. Ballarino, and L. Tora. 2011. Collisions between replication and transcription complexes cause common fragile site instability at the longest human genes. *Mol. Cell*. 44:966–977. http://dx.doi.org/10.1016/j.molcel.2011.10.013

Kannouche, P.L., J. Wing, and A.R. Lehmann. 2004. Interaction of human DNA polymerase eta with monoubiquitinated PCNA: a possible mechanism for the polymerase switch in response to DNA damage. *Mol. Cell*. 14:491–500. http://dx.doi.org/10.1016/S1097-2765(04)00259-X

Koo, H.-S., H.-M. Wu, and D.M. Crothers. 1986. DNA bending at adenine • thymine tracts. *Nature*. 320:501–506. http://dx.doi.org/10.1038/320501a0

Letessier, A., G.A. Millot, S. Koundrioukoff, A.M. Lachagès, N. Vogt, R.S. Hansen, B. Malfoy, O. Brison, and M. Debatisse. 2011. Cell-type-specific replication initiation programs set fragility of the FRA3B fragile site. *Nature*. 470:120–123. http://dx.doi.org/10.1038/nature09745

Lukas, C., V. Savic, S. Bekker-Jensen, C. Doil, B. Neumann, R.S. Pedersen, M. Grøfte, K.L. Chan, I.D. Hickson, J. Bartek, and J. Lukas. 2011. 53BP1 nuclear bodies form around DNA lesions generated by mitotic transmission of chromosomes under replication stress. *Nat. Cell Biol.* 13:243–253. http://dx.doi.org/10.1038/ncb2201

Lukusa, T., and J.P. Fryns. 2008. Human chromosome fragility. *Biochim. Biophys. Acta*. 1779:3–16. http://dx.doi.org/10.1016/j.bbagrm.2007.10.005

Masutani, C., R. Kusumoto, A. Yamada, N. Dohmae, M. Yokoi, M. Yuasa, M. Araki, S. Iwai, K. Takio, and F. Hanaoka. 1999. The XPV (xeroderma pigmentosum variant) gene encodes human DNA polymerase eta. *Nature*. 399:700–704. http://dx.doi.org/10.1038/21447

Matsuda, T., K. Bebenek, C. Masutani, I.B. Rogozin, F. Hanaoka, and T.A. Kunkel. 2001. Error rate and specificity of human and murine DNA polymerase eta. *J. Mol. Biol.* 312:335–346. http://dx.doi.org/10.1006/jmbi.2001.4937

McCulloch, S.D., R.J. Kokoska, C. Masutani, S. Iwai, F. Hanaoka, and T.A. Kunkel. 2004. Preferential cis-syn thymine dimer bypass by DNA polymerase eta occurs with biased fidelity. *Nature*. 428:97–100. http://dx.doi.org/10.1038/nature02352

Mirkin, S.M. 2007. Expandable DNA repeats and human disease. *Nature*. 447:932–940. http://dx.doi.org/10.1038/nature05977

Mishmar, D., A. Rahat, S.W. Scherer, G. Nyakatura, B. Hinzmann, Y. Kohwi, Y. Mandel-Gutfroind, J.R. Lee, B. Drescher, D.E. Sas, et al. 1998. Molecular characterization of a common fragile site (FRA7H) on human chromosome 7 by the cloning of a simian virus 40 integration site. *Proc. Natl. Acad. Sci. USA*. 95:8141–8146. http://dx.doi.org/10.1073/pnas.95.14.8141

Naim, V., and F. Rosselli. 2009. The FANC pathway and BLM collaborate during mitosis to prevent micro-nucleation and chromosome abnormalities. *Nat. Cell Biol.* 11:761–768. http://dx.doi.org/10.1038/ncb1883

Ozeri-Galai, E., R. Lebofsky, A. Rahat, A.C. Bester, A. Bensimon, and B. Kerem. 2011. Failure of origin activation in response to fork stalling leads to chromosomal instability at fragile sites. *Mol. Cell*. 43:122–131. http://dx.doi.org/10.1016/j.molcel.2011.05.019

Pearson, C.E., K. Nichol Edamura, and J.D. Cleary. 2005. Repeat instability: mechanisms of dynamic mutations. *Nat. Rev. Genet.* 6:729–742. http://dx.doi.org/10.1038/nrg1689

Rey, L., J.M. Sidorova, N. Puget, F. Boudsocq, D.S. Biard, R.J. Monnat Jr., C. Cazaux, and J.S. Hoffmann. 2009. Human DNA polymerase eta is required for common fragile site stability during unperturbed DNA replication. *Mol. Cell. Biol.* 29:3344–3354. http://dx.doi.org/10.1128/MCB.00115-09

Sabbioneda, S., A.M. Gourdin, C.M. Green, A. Zotter, G. Giglia-Mari, A. Houtsmuller, W. Vermeulen, and A.R. Lehmann. 2008. Effect of proliferating cell nuclear antigen ubiquitination and chromatin structure on the dynamic properties of the Y-family DNA polymerases. *Mol. Biol. Cell*. 19:5193–5202. http://dx.doi.org/10.1091/mbc.E08-07-0724

Schmutz, V., R. Janel-Bintz, J. Wagner, D. Biard, N. Shiomi, R.P. Fuchs, and A.M. Cordonnier. 2010. Role of the ubiquitin-binding domain of Polη in Rad18-independent translesion DNA synthesis in human cell extracts. *Nucleic Acids Res.* 38:6456–6465. http://dx.doi.org/10.1093/nar/gkq403

Schneider, B., S. Nagel, M. Kaufmann, S. Winkelmann, J. Bode, H.G. Drexler, and R.A. MacLeod. 2008. T(3;7)(q27;q32) fuses BCL6 to a non-coding region at FRA7H near miR-29. *Leukemia*. 22:1262–1266. http://dx.doi.org/10.1038/sj.leu.2405025

Schwartz, M., E. Zlotorynski, and B. Kerem. 2006. The molecular basis of common and rare fragile sites. *Cancer Lett.* 232:13–26. http://dx.doi.org/10.1016/j.canlet.2005.07.039

Shah, S.N., P.L. Opresko, X. Meng, M.Y. Lee, and K.A. Eckert. 2010. DNA structure and the Werner protein modulate human DNA polymerase delta-dependent replication dynamics within the common fragile site FRA16D. *Nucleic Acids Res.* 38:1149–1162. http://dx.doi.org/10.1093/nar/gkp1131

Sonoda, E., M.S. Sasaki, C. Morrison, Y. Yamaguchi-Iwai, M. Takata, and S. Takeda. 1999. Sister chromatid exchanges are mediated by homologous recombination in vertebrate cells. *Mol. Cell. Biol.* 19:5166–5169.

Strahs, D., and T. Schlick. 2000. A-tract bending: insights into experimental structures by computational models. *J. Mol. Biol.* 301:643–663. http://dx.doi.org/10.1006/jmbi.2000.3863

Takata, M., M.S. Sasaki, S. Tachiiri, T. Fukushima, E. Sonoda, D. Schild, L.H. Thompson, and S. Takeda. 2001. Chromosome instability and defective recombinational repair in knockout mutants of the five Rad51 paralogs. *Mol. Cell. Biol.* 21:2858–2866. http://dx.doi.org/10.1128/MCB.21.8.2858-2866.2001

Tourrière, H., and P. Pasero. 2007. Maintenance of fork integrity at damaged DNA and natural pause sites. *DNA Repair (Amst.).* 6:900–913. http://dx.doi.org/10.1016/j.dnarep.2007.02.004

Wang, G., and K.M. Vasquez. 2006. Non-B DNA structure-induced genetic instability. *Mutat. Res.* 598:103–119. http://dx.doi.org/10.1016/j.mrfmmm.2006.01.019

Xie, B., N. Mazloum, L. Liu, A. Rahmeh, H. Li, and M.Y. Lee. 2002. Reconstitution and characterization of the human DNA polymerase delta four-subunit holoenzyme. *Biochemistry.* 41:13133–13142. http://dx.doi.org/10.1021/bi0262707

Zhang, H., and C.H. Freudenreich. 2007. An AT-rich sequence in human common fragile site FRA16D causes fork stalling and chromosome breakage in *S. cerevisiae*. *Mol. Cell.* 27:367–379. http://dx.doi.org/10.1016/j.molcel.2007.06.012

Zou, L., D. Cortez, and S.J. Elledge. 2002. Regulation of ATR substrate selection by Rad17-dependent loading of Rad9 complexes onto chromatin. *Genes Dev.* 16:198–208. http://dx.doi.org/10.1101/gad.950302